Single-Atom Alloy Formation via Reaction Driven Catalyst Restructuring

Georgios Giannakakis,^{a,‡} Yogita Soni,^{a‡} Gregory L. Novotny,^{a,‡} Zhaoru Zha,^{a,‡} Nicole J. LiBretto,^b Yan-liu Dang,^c Steven L. Suib,^{c,d} Jeffrey T. Miller,^b E. Charles H. Sykes,^e Prashant Deshlahra^{a,*}

- ^a Department of Chemical and Biological Engineering, Tufts University, Medford, Massachusetts 02155, United States
- ^b Davidson School of Chemical Engineering, Purdue University, West Lafayette, Indiana 47907, United States
- c Institute of Materials Science, University of Connecticut, Storrs, Connecticut 06269, USA
- d Department of Chemistry, University of Connecticut, Storrs, Connecticut 06269, USA
- ^e Department of Chemistry, Tufts University, Medford, MA 02155, United States

Supporting Information Placeholder

ABSTRACT: We demonstrate that single-atom alloy catalysts can be made by exposing physical mixtures of monometallic Cu and Pd supported catalysts to vinyl acetate synthesis reaction conditions. This reaction induces the formation of mobile clusters of metal diacetate species that drive extensive metal nanoparticle restructuring leading to atomic dispersion of the precious metal, smaller nanoparticle sizes than the parent catalysts, and high activity and selectivity for both vinyl acetate synthesis and ethanol dehydrogenation reactions. This approach is scalable and appears to be generalizable to other alloy catalysts.

Introduction

Vinyl acetate (VA) is an important chemical prooxidative ethylene acetoxylation $(CH_{3}COOH + C_{2}H_{4} + \frac{1}{2}O_{2} \rightarrow CH_{3}COOC_{2}H_{3} + H_{2}O)$ on Pd-based heterogenous catalysts (e.g., K-Pd₂Au/SiO₂).¹⁻⁸ These catalysts are however prone to metal leaching via the formation of mobile clusters of diacetate species [e.g., Pd₃(OAc)₆].9 Here, we show that this diacetate-mediated dynamical catalyst restructuring can be harnessed to synthesize new alloy structures with superior properties. Specifically, monometallic catalysts containing Pd and Cu nanoclusters with micron-scale separation restructure extensively and achieve full dispersion of Pd atoms in the Cu surface when exposed to VA synthesis conditions, and subsequently form single-atom alloys (SAAs) when reduced back to metallic form via H2 treatment.

SAAs containing precious metals dispersed as isolated atoms within the lattice of a less active host¹⁰ can exhibit improved reactivity, selectivity and stability over their monometallic counterparts for a variety of important reactions.^{11, 12} For VA synthesis, dilution of Pd by Au¹³ and pairs of isolated Pd-atoms^{14, 15} have been proposed to enhance activity. Very few studies involving catalyst compositions other than monometallic Pd and bimetallic PdAu have been reported for VA synthesis.

In this study, we probe PdCu as an alternative catalyst due to the proposed importance of non-contiguous Pd atoms in the reaction, and the intrinsic thermodynamic stability of atomically dispersed Pd in Cu.16, 17 In doing so, we examine how VA formation rate and selectivity in physical mixtures of Pd/SiO₂ and Cu/SiO₂ catalysts as a function of time and reaction conditions compare with monometallic Pd/SiO₂ and co-impregnated bimetallic PdCu/SiO₂ catalysts. The transients in rates and selectivity upon initial exposure to VA synthesis conditions suggest a catalyst restructuring, which is studied further using microscopy, x-ray absorption spectroscopy, diffuse reflection infrared spectroscopy of bound CO molecules and ethanol dehydrogenation catalysis. These analyses reveal that reduction of the catalysts restructured by VA synthesis reaction leads to SAA nanoparticles with atomic dispersion of Pd in Cu and much smaller sizes than nanoparticles that existed before the exposure to VA synthesis reaction conditions. Transmission infrared spectroscopy demonstrating the formation of mobile diacetate species under VA synthesis reaction conditions and the effects of parameters such as initial distance between Pd and Cu nanoparticles and reaction conditions on the extent of restructuring are studied to understand how this restructuring process can be utilized for preparing efficient SAA catalysts.

Results and Discussion

Figure 1 compares the VA formation rate and VA selectivity on (i) an SiO_2 -supported Pd catalyst, (ii) a bimetallic catalyst with 0.03:1 Pd:Cu atomic ratio synthesized by co-impregnation with premixed precursor solution (Pd $_{0.03}$ Cu), and (iii) a physical mixture of separately prepared monometallic catalyst powders (0.03Pd+Cu). To prepare the physical mixtures, 1wt.%Pd/SiO $_2$ and 5wt.%Cu/SiO $_2$ samples prepared by incipient wetness impregnation are thoroughly mixed using a mortar and pestle as described in Supporting Information (SI, Section S1). The SiO $_2$ powders were comprised of 40-74 μ m aggregates and were not pressed to achieve larger aggregates after impregnation or mixing unless stated otherwise.

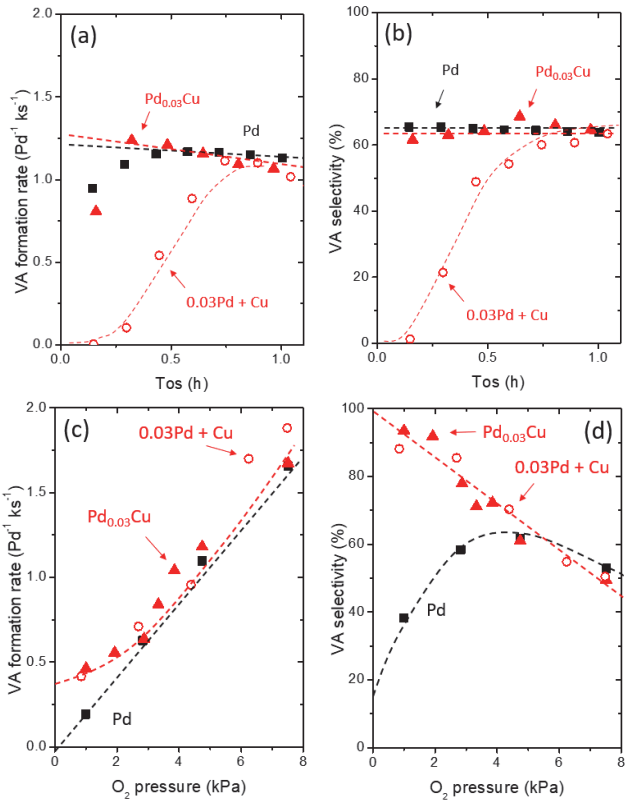


Figure 1. (a,c) VA formation rate and (b,d) VA selectivity on SiO_2 supported 1wt.%Pd, $4wt.\%Pd_{0.03}Cu$ and 4.2wt.%0.03Pd+Cu (physical mixture) as a function of time on stream at 5kPa O_2 (a, b), and of O_2 pressure (c, d). Conditions: $160^{\circ}C$, 40kPa C_2H_4 , 10kPa CH_3COOH , $40cm^3min^{-1}$ flow, <10% conversion of all reactants. Dashed lines represent trends.

At short times after introducing VA synthesis reactants (40, 10, 5 kPa C₂H₄, CH₃COOH, O₂), the rate and selectivity for co-impregnated Pd_{0.03}Cu is similar to Pd (**Figs. 1a-b**, 1.2Pd⁻¹s⁻¹ and 65%). In contrast, the rate and VA selectivity are initially near-zero on the 0.03Pd+Cu physical mixture catalyst but increase dramatically to values near Pd_{0.03}Cu within 1h. Beyond the initial transients, Pd_{0.03}Cu and 0.03Pd+Cu samples exhibit nearly identical performance. Both bimetallic samples, however, differ from monometallic Pd at low O_2 pressures. The rates decrease linearly with O_2 pressure on Pd but become less sensitive to pressure on $Pd_{0.03}Cu$ and 0.03Pd+Cu at low pressures (**Fig. 1c**). More significantly, VA selectivity on Pd decreases with pressure below 4 kPa to approach values near 20% in the 0 kPa limit, but it increases on Pd_{0.03}Cu and 0.03Pd+Cu samples to approach 100% (Fig. 1d), indicating the much superior catalytic properties of the bimetallic samples at these conditions.

Catalysts involving multiple active site components are often compared to physical mixtures of their individual components in order to probe the importance of site proximity. The near identical rate and selectivity trends for the P_{0.03}Cu alloy and 0.03Pd+Cu physical mixture samples (**Fig. 1c-d**) would initially suggest that atomic Pd-Cu contact is not required for promotional effects of Cu unless the catalysts restructured to achieve atomic contact even in the physical mixture. However, as shown in **Figure 1a-b**, the initial transients for the physical mixture indicate that the catalyst may indeed have restructured within 1h of the measurement. We next probe this surprisingly extensive restructuring via microscopic and spectroscopic methods.

Transmission electron microscopy (TEM) and energy dispersive spectroscopy (EDS) were used to examine elemental distributions indicative of particle migration between Pd/SiO₂ and Cu/SiO₂ particles in physical mixtures, as well as the nanoparticle sizes in co-impregnated catalysts, physical mixtures, and monometallic Pd/SiO₂. Figure 2a shows a high-angle annular dark field (HAADF) scanning TEM (STEM) image of a SiO₂ particle in the 0.03Pd+Cu physical mixture sample after "VA treatment" (exposure to 40, 10, 5 kPa C₂H₄, CH₃COOH, O₂ at 160°C for 2h, followed by treatment in H₂ at 400°C for 0.5h). The corresponding EDS maps show that both Cu and Pd are present on the same SiO₂ particle (Fig.2 b-c), suggesting that metal atoms moved across the micron-scale distances between SiO₂ particles in the mixture of Pd/SiO₂ and Cu/SiO₂. **Figures 2d** and **2e** show TEM images of the co-impregnated Pd_{0.03}Cu sample before and after the VA treatment, respectively. The mean particle diameter of this sample decreases from 22±8nm to 14±6nm

sample upon the VA treatment. The particle size also decreases significantly with VA treatment for the 0.03Pd+Cu physical mixture sample as confirmed by x-ray diffraction peak widths and the Scherrer equation (average Cu size 42nm and 12nm before and after VA; Fig. S3, Table S3) and by TEM (16±5nm after VA Fig. S5a). Notably, the high-resolution TEM images show that nanoparticles exhibit irregular shapes indicative of agglomerates of smaller domains, suggesting that effective particle sizes are smaller than that detected from TEM (Fig. S5b-c). This particle size decrease is not a result of metal loss by VA treatment, which we confirmed using inductively coupled plasma based elemental analysis (Table S2). Monometallic Pd/SiO₂ samples also exhibit a large increase in the number of small nanoparticles (<3 nm; Fig. S4). These changes suggest that exposure to vapor-phase VA synthesis reaction conditions drastically restructures the nanoparticles via movement of metal atoms across micrometer scales for physical mixtures and nanometer scales for co-impregnated and monometallic samples.

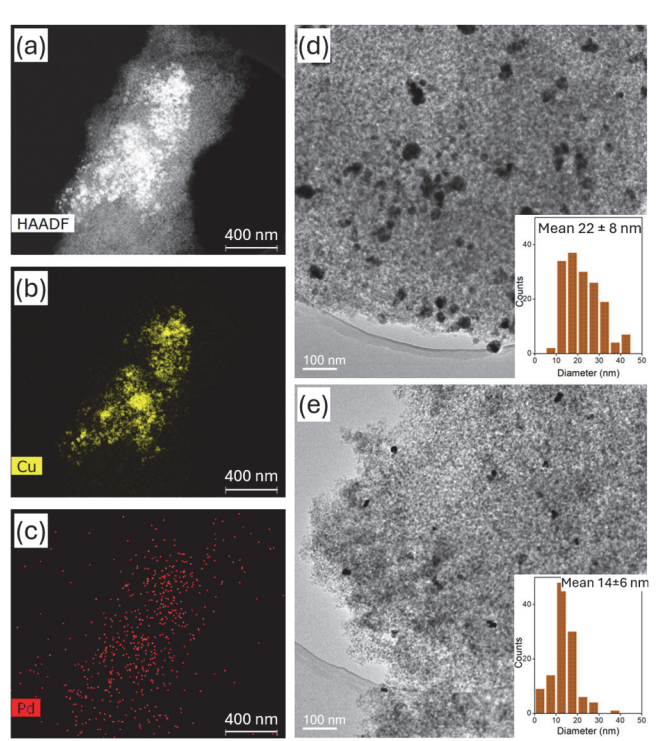


Figure 2. (a) HAADF image and (b) Cu and (c) Pd elemental maps after VA treatment for 4.2wt.%0.03Pd+Cu (physical mixture) sample, and TEM images and nanoparticle size distributions for 4 wt.% Pd_{0.03}Cu co-impregnated sample (d) before and (e) after VA treatment (40, 10, 5 kPa C₂H₄, CH₃COOH, O₂, 160°C for 2h, followed by treatment in H₂ at 400°C for 0.5 h).

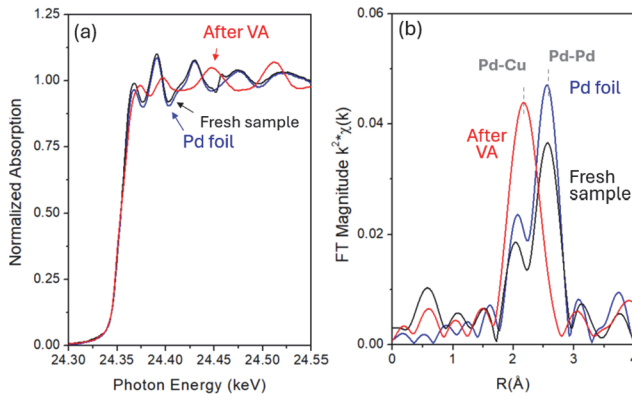


Figure 3. (a) Normalized X-ray absorption spectra and (b) magnitudes of Fourier transforms at the Pd K edge for 4.2 wt.% 0.03 Pd + Cu (physical mixture) before and after VA treatment (40, 10, 5 kPa C₂H₄, CH₃COOH, O₂, 160°C , 2h). All samples were treated in H₂ at 400°C prior to measurements.

Table 1. Scattering path, coordination number (CN), and nearest-neighbor distances ($R_{\rm EXAFS}$, $R_{\rm DFT}$) for 4.2wt.%0.03Pd+Cu sample before and after VA treatment. ^a

| Sample | Scattering Path ^b | CN b | R _{EXAFS} b (Å) | R _{DFT} ^c (Å) |
|----------|------------------------------|------|--------------------------|-----------------------------------|
| Fresh | Pd-Pd | 10.8 | 2.73 | 2.79 |
| | Cu-Cu | 9.5 | 2.56 | 2.57 |
| After VA | Pd-Cu | 10.9 | 2.58 | 2.59-2.61 |
| | Cu-Cu | 8.8 | 2.56 | 2.57 |

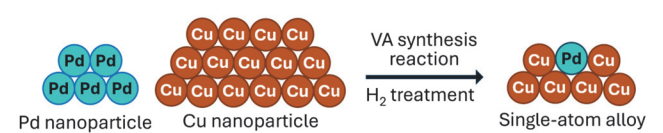
 $^{^{\}rm a}$ Treatment conditions: 40, 10, 5 kPa C₂H₄, CH₃COOH, O₂, 160°C, 2h, followed by H₂ treatment at 400 °C

Next, we used x-ray absorption spectroscopy to probe average local environment of Pd and Cu atoms in fresh and VA treated samples. Figure 3 compares spectra at the Pd-K-edge in the physical mixture in asprepared form (fresh), and after VA treatment. The fresh sample matches a Pd foil and exhibits only Pd-Pd coordination, but after VA treatment only Pd-Cu coordination is detected. The corresponding spectra for the Cu-K-edge are in SI (Fig. S9) and show Cu-Cu coordination before and after VA treatment. Table 1 shows the atomic coordination numbers and nearestneighbor distances determined by fitting extended xray absorption fine structure data (EXAFS) and nearest-neighbor distances from density functional theory (DFT) calculations (details in SI, XAS: Figs. S7-S10, Tables S4-S5; DFT: Fig. S22, Table S8). The coordination numbers exhibit values ranging from 11 to 8.8, suggesting nanoparticles below 10 nm,¹⁹ which is smaller than average sizes for bimetallic samples determined from TEM and XRD. This difference likely reflects the irregular and fragmented shapes of Cu

b derived from EXAFS fitting at Pd and Cu K edges (Figs. S7-S10, Tables S4-S5)

c derived from DFT calculations (Fig. S22, Table S8)

particles in high resolution TEM (**Fig. S5b-c**) and the inability to sample small particles in XRD. The decrease in Cu-Cu coordination (**Table 1**) is consistent with a decrease in particle size after VA treatment. The Pd-Pd, Pd-Cu and Cu-Cu distances from EXAFS fitting are consistent with trends in our DFT values and with the literature, indicating that Pd-Cu distances in dilute alloys are much closer to bulk Cu-Cu distances than an average of bulk Cu-Cu and bulk Pd-Pd distances.²⁰ EXAFS analysis is also performed for a Pd_{0.036}Cu co-impregnated sample, which also shows an increased Pd-Cu coordination and a decreased in Cu-Cu coordination after VA treatment (**Tables S4-S5**), which is consistent with improved atomic dispersion of Pd and decrease in bimetallic particle size.



Scheme 1. Restructuring of physical mixture sample via VA treatment.

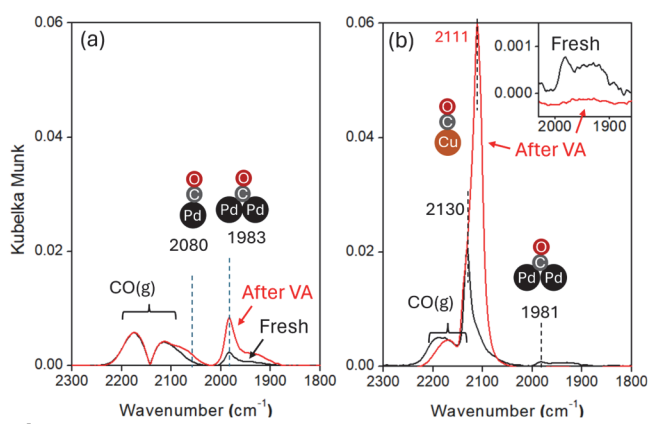


Figure 4. CO-DRIFTS spectra in 1%CO at 150°C before and after VA treatment for (a) 1wt.%Pd/SiO₂, and (b) 4.2wt.%0.03Pd+Cu (physical mixture) before and after VA treatment (40, 10, 5 kPa C₂H₄, CH₃COOH, O₂, 160°C, 2h). Samples were treated in H₂ at 400°C prior to measurements. Inset in (b) expands the DRIFTS spectra in the region of CO at Pd-Pd bridges.

Microscopy and EXAFS results show the formation of smaller nanoparticles and alloying of Pd with Cu via increase in average coordination numbers that sample both surface and bulk atoms (**Scheme 1**). We next turn to diffuse reflectance infrared Fourier transform spectra (DRIFTS) of adsorbed CO molecules as a probe of Pd-Pd coordination specifically in exposed surfaces of nanoparticles. **Figure 4** shows CO-DRIFTS spectra before and after VA treatment for monometallic Pd/SiO₂ and 0.03Pd+Cu physical mixture catalysts. The fresh monometallic sample exhibits a peak at 1983 cm⁻¹ corresponding to CO molecules adsorbed at Pd-Pd

bridging positions,^{21, 22} and a weak shoulder near the gaseous CO features at 2080 cm-1 that reflects CO adsorbed atop Pd atoms (Fig. 4a). After VA treatment, these features become more intense, which is consistent with the increased number for smaller Pd nanoparticles in TEM images that expose more surface Pd sites (Fig. S4). The physical mixture sample exhibits peaks at 2130 cm⁻¹ and 1981 cm⁻¹ that corresponds to CO molecules atop Cu atoms and at Pd-Pd bridges, respectively (Fig. 4b). In contrast to the monometallic sample, the 1981 cm⁻¹ peak in the physical mixture disappears after VA treatment, which shows the elimination of Pd-Pd coordination due to the formation of Pd-Cu SAA. The 2130 cm⁻¹ peak becomes more intense and shifts to 2111 cm⁻¹ after VA treatment. The higher intensity suggests the formation of smaller particles that expose more Cu atoms, while the shift to lower wavenumbers is typically attributed to changes in partial Cu charge ($Cu^{\delta+}$ to Cu^0)²³ or low-coordinated Cu sites.24

SAAs are sensitive to dilute atom segregation and aggregation in response to CO exposure and treatment temperature.^{25, 26} Therefore, DRIFTS measurements were also performed at room temperature to eliminate any CO mediated restructuring at 150°C, as shown in SI (**Figs. S12-S15**). These spectra also show the disappearance of signals corresponding to Pd-Pd bridge-bound CO after VA treatment, consistent with the SAA formation.

We further probed the catalytic properties of the SAAs formed by VA treatment using non-oxidative endothermic ethanol dehydrogenation as a highly site-sensitive probe reaction. Specifically, extensive studies on Au and Cu based SAA catalysts have shown that even small ensembles of the active metal atoms can promote undesired decomposition reactions over selective ethanol dehydrogenation.^{25, 27-31} Therefore, small Pd clusters below the detection limit of our EXAFS or CO-DRIFTS experiments can be still be probed by monitoring the selectivity of the ethanol dehydrogenation reaction.³²

We found that monometallic Pd samples exhibited a low dehydrogenation rate and selectivity, which remained low after VA treatment (**Fig. 5a**, 0.12 vs. 0.23 Pd⁻¹s⁻¹ rate, 11% vs. 23% selectivity before vs. after VA treatment). The physical mixture 0.03Pd+Cu catalyst exhibits moderate rates and selectivity in its fresh form (7 Pd⁻¹s⁻¹, 55%), but after VA treatment the rate increases fourfold (30 Pd⁻¹s⁻¹) and selectivity increases to 99.3%. With these large rate and selectivity enhancements the ethanol conversion increases significantly to nearly 80% of the equilibrium limit for the endothermic dehydrogenation reaction at 200°C (definition in SI, **Eq. S1**). The 80% approach to

equilibrium (η) suggests that the forward rate of formation of acetaldehyde is about 5 times the 30 Pd-1s-1 value shown in **Figure 5a** [and 20 times rate on fresh 0.03Pd+Cu; (forward rate) = (net rate)× $(1 - \eta)$ Eq. **S2**]. This high rate and near 100% selectivity to acetaldehyde at near-equilibrium conversions reflect smaller nanoparticle sizes and a complete atomic dispersion of Pd in Cu which leads to efficient utilization of the precious metal. The fresh Pd_{0.03}Cu sample exhibits a higher rate and selectivity than fresh physical mixture (Fig. 5a, 22 Pd-1s-1, 96.6%) because the co-impregnation disperses Pd in Cu to a significant extent. Even for this alloyed sample, however, the rate and selectivity improve further after VA treatment (Fig. 5a, 32 Pd⁻¹s⁻¹, 98.3% selectivity at 83% of equilibrium conversion), consistent with the improved atomic dispersion and smaller Cu nanoparticle size it induces. The high selectivity at high conversion reflects the ability of the SAAs to activate C-H bonds in C2H5OH efficiently, and the oxophilic Cu atoms promoting adsorption configurations of the product CH₃CHO that inhibits unselective C-C scission (Fig. 5b).³³ Monometallic Cu samples also exhibit essentially 100% selectivity but with rates much lower and conversions far from equilibrium at comparable conditions (**Table S6**, Fig. S16b), highlighting the importance of the Pd dopant atoms and their high dispersion as induced by the VA treatment.

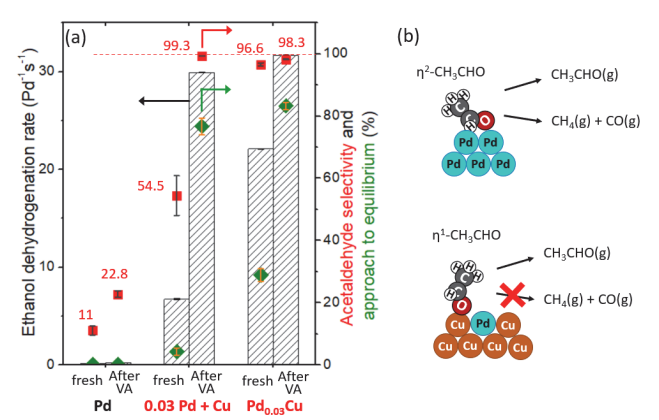


Figure 5. (a) CH₃CHO formation rate, selectivity, and approach to equilibrium for C_2H_5OH dehydrogenation on 1wt.%Pd, physical mixture 4.2wt.%(0.03Pd+Cu), and coimpregnated 4wt.%Pd_{0.03}Cu at 200°C, 2kPa C_2H_5OH and 40 cm³ min⁻¹ flow before and after exposure to VA synthesis conditions (160°C, 40kPa C_2H_4 , 10kPa C_1H_4). All samples were treated in H_2 at 400°C before measurements. (b) CH₃CHO adsorption configurations and secondary products on contiguous Pd-Pd sites vs. isolated Pd atoms.

Physical mixtures with higher Pd:Cu atomic ratios (0.2Pd+Cu) also restructure extensively via VA

treatment, leading to smaller alloyed particles (**Table S3**), no detectable bridge-bonded CO characteristic of Pd-Pd ensembles (**Figs. S11, S14**), and much higher ethanol dehydrogenation rate and selectivity than the fresh sample (**Fig. S16**). However, the selectivity was 93% (vs. 99.3% for 0.03Pd) even at only 30% of the equilibrium conversion, suggesting that some aggregated Pd ensembles below the detection limit of the CO-DRIFTS measurements must be present in the higher Pd loading 0.2Pd+Cu sample. These findings demonstrate that the ethanol dehydrogenation reaction itself is more sensitive than CO-DRIFTS or EXAFS in detecting the trace amounts of Pd ensembles that perform unselective chemistry.

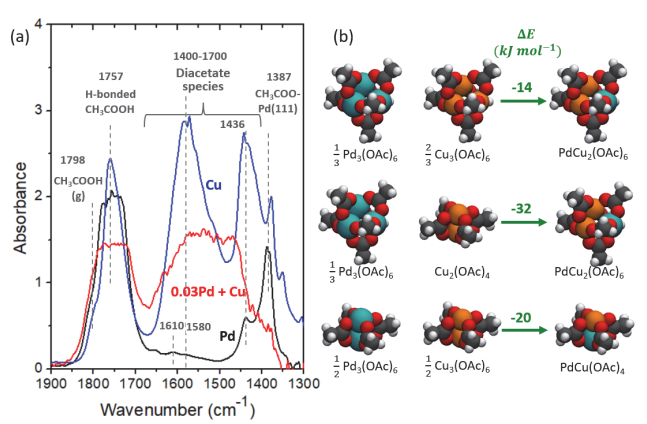


Figure 6. (a) *In situ* transmission IR spectra of acetate species on 1wt.%Pd, 5wt.%Cu and 4.2wt.%(0.03Pd+Cu) at 160° C, 10kPa C_{2} H₄, 5kPa C_{3} COOH, 5kPa O_{2} , and (b) Reaction energies for Pd and Cu diacetate species to form mixed diacetate species.

Next, we probe the identity of intermediate species involved in the restructuring of physical mixtures using in situ transmission infrared (IR) spectroscopy and DFT calculations. Acetic acid and different types of acetate species exhibit C-O stretching absorption bands in the 1200-1800 cm⁻¹ range. **Figure 6a** shows spectra for Pd, Cu and 0.03Pd+Cu samples under VA synthesis conditions. The peak assignments for these spectra are derived from comparing measured spectra on SiO₂ powder without metals and on Pd/SiO₂ sample under different conditions with spectra generated from DFT-derived frequencies and dipole moments shown in SI (Fig. S20). All three samples show features for gaseous and H-bonded CH₃COOH with the latter being much more abundant (1700-1800 cm⁻¹). Monometallic Pd and Cu exhibit peaks for acetates adsorbed on the metal surface (1387 cm⁻¹).³⁴ Small quantities of diacetate species form on the Pd sample at 1610 and 1580 cm⁻¹ when exposed to a CH₃COOH-O₂ mixture, but C₂H₄ in VA synthesis conditions essentially eliminates those peaks (SI, Fig. S20). In contrast, monometallic Cu exhibits strong diacetate peaks. The 0.03Pd+Cu physical mixture differs from both Pd and Cu by showing essentially no metal adsorbed acetates and broader spectral features than Cu in the diacetate region (Fig. 6a). The reaction energies shown in Figure 6b thermodynamically favor the formation of mixed PdCu diacetates (in trimer and dimer forms) from Pd and Cu diacetates, and DFT derived spectra for such mixed diacetates are broader than that for Cu only (Fig. S21b). Taken together, these results indicate that Cu diacetate formation is thermodynamically more favorable than Pd diacetate, which leads to a greater equilibrium concentration of the former species under identical conditions for the corresponding monometallic samples. The thermodynamic driving force for diacetate formation is further enhanced by the greater stability of mixed PdCu diacetates, which eliminates essentially all metal-bound acetate species and makes mixed-metal diacetate clusters the most abundant species under reaction conditions. Mixedmetal diacetate clusters exhibit more diverse structures, leading to broader spectral features and no metallic nanoparticles with adsorbed acetate when both Pd and Cu are present.

The molecular nature of diacetates enables their motion across the network of highly abundant physisorbed H-bonded acetic acid (1757 cm $^{-1}$, **Fig. 6a**) between SiO₂ particles.³⁵ ³⁶ Pd and Cu diacetates are known to decompose before melting or vaporizing,³⁷, ³⁸ which suggests that a reactive environment is needed to repeatedly reform these species during restructuring. Under these conditions, the mobility would require solvation of diacetate clusters by acetic acid layers and some connectivity in these layers across SiO₂ particles would be expected.

To probe the length scales over which effective restructuring can be achieved, we compared post-VAtreatment C₂H₅OH dehydrogenation reaction rate and selectivity in the co-impregnated sample and the standard physical mixture (40-74 µm) to physical mixtures of larger aggregates of Pd/SiO2 and Cu/SiO2 (180-300 µm). These comparisons are shown in SI (Fig. S23) and indicate that the larger particles still exhibit significant enhancement over fresh physical mixtures, but the enhanced rates are lower than that for smaller particles, and selectivity is also slightly lower despite being further away from equilibrium. Thus, it appears that these larger SiO₂ particles lead to less effective restructuring due to limitations in the transport of diacetate species across the larger distances.

Changes in the effectiveness of restructuring with deviations from the standard VA treatment conditions $(40, 10, 5 \text{ kPa C}_2\text{H}_4, \text{CH}_3\text{COOH}, \text{O}_2)$ were also examined

by measuring post-treatment ethanol dehydrogenation reaction rate and selectivity as shown in SI (Fig. **S18**). Lower O_2 pressures (1 or 0 kPa O_2) lead to significantly lower C₂H₅OH dehydrogenation rates and slightly lower selectivity that suggest less complete restructuring. In contrast, eliminating C₂H₄ gives high rates even at low O₂ pressure (**Fig. S18**). C₂H₄ acts as a reductant, which decreases the concentration of oxidized diacetate species, as can be seen from in situ IR spectra in SI (Fig. S20b) and is consistent with effect of C₂H₄ pressure on acetate coverage in kinetic studies³⁹ Thus, reaction conditions without C₂H₄ that enhance diacetate formation also enhance restructuring. These tests indicate that not all three reactants involved in VA synthesis are required for restructuring but they each provide independent parameters with which to control restructuring. While CH₃COOH -O₂ treatment is sufficient for the synthesis of Pd-Cu SAA catalysts, we hypothesize that C₂H₄ maybe be harnessed to moderate leaching by decomposing diacetates in systems in which these species are more mobile or volatile.

When both Pd and Cu are present the IR spectra show mainly diacetate bands with very little intensity at the wavenumbers corresponding to acetates bound to metal nanoparticles (Fig. 6a). This enhanced diacetate formation, together more complete restructuring under conditions of higher diacetate formation (Fig. S18) and the DFT-derived higher stability of mixed diacetate clusters (Fig. 6b), suggests that the restructuring is particularly effective for systems with stable mixed diacetates. However, the ultimate thermodynamic stability of the alloys formed via H₂ treatment of diacetates also matters. Pd and Cu are well known to form stable alloys, which is also confirmed by our DFT calculations (SI, Table S8). At sufficiently low loadings, the method presented here may also allow bimetallic nanoparticles of metals with less favorable mixing enthalpies but stable mixed diacetates by trapping them in metastable states during the reductive treatment. More work is needed to identify systems with suitable metallic and diacetate mixing energetics, as well as to optimize treatment conditions and metal loadings to achieve uniform nanoparticle sizes. Some of the readily apparent advantages of the diacetate mediated method for SAA formation include, (i) avoidance of the need to reduce oxophilic hosts such as Cu to metallic form before addition of dopants, which is needed for alternative methods such as galvanic replacement but is challenging to achieve under aqueous conditions of such synthesis (ii) ability to redistribute dopants in previously synthesized catalysts with poor distribution or degradation or segregation under harsh conditions, (iii) the potential to break-up monometallic particles that have a high cohesive energy but are ultimately stable in bimetallic form after the redistribution.

Conclusions

We demonstrate that vapor phase VA synthesis conditions involving acetic acid, oxygen, and ethylene extensively restructure pure Pd and Cu nanoparticles and form small SAA nanoparticles with full atomic dispersion of Pd in Cu, negating the need for complex solution-based synthesis. This new method for SAA formation greatly enhances the rate and selectivity of PdCu for both the VA synthesis and ethanol dehydrogenation reaction. The restructuring itself is mediated by mobile clusters of diacetate species with cationic metal atoms, suggesting that the stability and mixing energies of these diacetate species can be used to generalize the applicability of these methods in SAA catalyst design. Such reaction induced metal restructuring should have broad applications e.g. recovering site isolated catalysts from non-uniform alloys formed by other methods or harsh reaction conditions or offering a scalable alternative to more complex batch synthesis of SAA catalysts.

ASSOCIATED CONTENT

Supporting Information. The Supporting Information is available free of charge at the ACS Publications website.

Catalyst Synthesis Methods; Rate and Selectivity Measurements; Elemental Analysis; X-ray Diffraction, Microscopy and X-ray Absorption Measurements; CO-DRIFTS Measurements 150°C and Room Temperature; Effect of Sample Composition, VA Treatment Conditions and SiO₂ Particle Size Effects on C₂H₅OH Dehydrogenation Rate and Selectivity; Computational Methods; DFT-Derived Stability and IR spectra of Metal Diacetate Species and Stability of SAAs; Transmission IR Spectroscopy Under VA Synthesis Reaction Conditions and Mechanism of Catalyst Restructuring. (PDF)

AUTHOR INFORMATION

Corresponding Author

Prashant Deshlahra - Department of Chemical and Biological Engineering, Tufts University, Medford, Massachusetts 02155, United States; ORCID: 0000-0002-1063-4379; Email: prashant.deshlahra@tufts.edu

Author Contributions

‡GG, YS, GLN and ZZ contributed equally to this work. All authors have given approval to the final version of the manuscript.

Notes

The authors declare no competing financial interest.

ACKNOWLEDGMENT

We thank Dr. Junkai He (UCONN), Ms. Chathupama Jayasinghe (UCONN), and Mr. Ho Yi Lam (Tufts) for assistance with microscopy, XRD, and ICP measurements. This work was funded by NSF CAREER award (grant# 2045675). Computational resources were provided by Advanced Cyberinfrastructure Coordination Ecosystem: Services & Support (ACCESS), which is supported by NSF.⁴⁰ CS thanks the US Department of Energy, Basic Energy Sciences, CPIMS program, under grant# DE-SC0004738. SLS acknowledges the support of the Center for Advanced Microscopy and Materials Analysis.

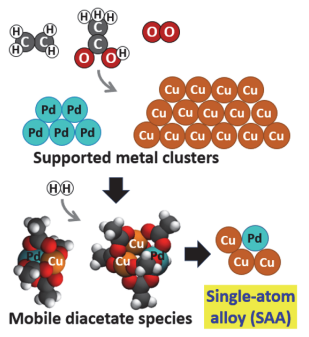
REFERENCES

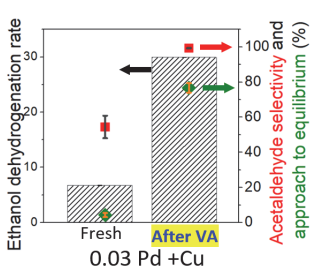
- (1) Kumar, D.; Chen, M.; Goodman, D. Synthesis of Vinyl Acetate on Pd-Based Catalysts. *Catalysis today* **2007**, *123* (1-4), 77-85.
- (2) Nakamura, S.; Yasui, T. Formation of Palladous Acetate and Stability of Catalyst in Palladium-Metal-Catalyzed Synthesis of Vinyl Acetate From Ethylene. *Journal of Catalysis* **1971**, *23* (3), 315-320.
- (3) Han, Y.-F.; Kumar, D.; Sivadinarayana, C.; Clearfield, A.; Goodman, D. The Formation of PdC_x Over Pd-Based Catalysts in Vapor-Phase Vinyl Acetate Synthesis: Does a Pd-Au Alloy Catalyst Resist Carbide Formation? Catalysis letters **2004**, *94*, 131-134.
- (4) Nakamura, S.; Yasui, T. The Mechanism of the Palladium-Catalyzed Synthesis of Vinyl Acetate From Ethylene in a Heterogeneous Gas Reaction. *Journal of Catalysis* **1970**, *17* (3), 366-374.
- (5) Hanrieder, E. K.; Jentys, A.; Lercher, J. A. Atomistic Engineering of Catalyst Precursors: Dynamic Reordering of PdAu Nanoparticles During Vinyl Acetate Synthesis Enhanced by Potassium Acetate. *ACS Catalysis* **2015**, *5* (10), 5776-5786.
- (6) Jacobs, H. P.; Elias, W. C.; Heck, K. N.; Dean, D. P.; Dodson, J. J.; Zhang, W.; Hong, K.; Arredondo, J. H.; Breckner, C. J.; Chen, L. Promotional Role of Acid Sites on Aluminosilicate-Supported PdAu for Vinyl Acetate Synthesis. *ACS Catalysis* **2023**, *14* (1), 211-226.
- (7) Nakaya, Y.; Hayashida, E.; Shi, R.; Shimizu, K.-i.; Furukawa, S. Interstitial Carbon Dopant in Palladium—Gold Alloy Boosting the Catalytic Performance in Vinyl Acetate Monomer Synthesis. *Journal of the American Chemical Society* **2023**, *145* (5), 2985-2998.
- (8) Calaza, F.; Stacchiola, D.; Neurock, M.; Tysoe, W. T. Coverage Effects on the Palladium-Catalyzed Synthesis of Vinyl Acetate: Comparison Between Theory and Experiment. *Journal of the American Chemical Society* **2010**, 132 (7), 2202-2207.
- (9) Stoyanov, E. IR Study of the Structure of Palladium (II) Acetate in Chloroform, Acetic Acid, and Their Mixtures in Solution and in Liquid-Solid Subsurface Layers. *Journal of Structural Chemistry* **2000**, *41* (3), 440-445.
- (10) Kyriakou, G.; Boucher, M. B.; Jewell, A. D.; Lewis, E. A.; Lawton, T. J.; Baber, A. E.; Tierney, H. L.; Flytzani-Stephanopoulos, M.; Sykes, E. C. H. solated Metal Atom Geometries as a Strategy for Selective Heterogeneous Hydrogenations. *Science* **2012**, *335* (6073), 1209-1212.
- (11) Hannagan, R. T.; Giannakakis, G.; Flytzani-Stephanopoulos, M.; Sykes, E. C. H. Single-Atom Alloy Catalysis. *Chemical Reviews* **2020**, *120* (21), 12044-12088.
- (12) Giannakakis, G.; Flytzani-Stephanopoulos, M.; Sykes, E. C. H. Single-Atom Alloys as a Reductionist Approach to the Rational Design of

- Heterogeneous Catalysts. Accounts of chemical research 2018, 52 (1), 237-247
- (13) Calaza, F.; Li, Z.; Garvey, M.; Neurock, M.; Tysoe, W. T. Reactivity and Selectivity in the Au/Pd (111) Alloy-Catalyzed Vinyl Acetate Synthesis. *Catalysis letters* **2013**, *143*, 756-762.
- (14) Chen, M.; Kumar, D.; Yi, C.-W.; Goodman, D. W. The Promotional Effect of Gold in Catalysis by Palladium-Gold. *Science* **2005**, *310* (5746), 291-293.
- (15) Garcia-Mota, M.; Lopez, N. Template effects in vinyl acetate synthesis on PdAu surface alloys: a density functional theory study. *Journal of the American Chemical Society* **2008**, *130* (44), 14406-14407.
- (16) Liu, Q.; Wang, X.; Li, L.; Song, K.; Wang, Y.; Qian, P. Catalytic Activity, Thermal Stability and Structural Evolution of PdCu Single-Atom Alloy Catalysts: The Effects of Size and Morphology. *RSC advances* **2022**, *12* (1), 62-71.
- (17) Shan, J.; Giannakakis, G.; Liu, J.; Cao, S.; Ouyang, M.; Li, M.; Lee, S.; Flytzani-Stephanopoulos, M. PdCu Single Atom Alloys for the Selective Oxidation of Methanol to Methyl Formate at Low Temperatures. *Topics in Catalysis* **2020**, *63*, 618-627.
- (18) Oenema, J.; Harmel, J.; Vélez, R. P. r.; Meijerink, M. J.; Eijsvogel, W.; Poursaeidesfahani, A.; Vlugt, T. J.; Zečević, J.; De Jong, K. P. Influence of Nanoscale Intimacy and Zeolite Micropore Size on the Performance of Bifunctional Catalysts for N-Heptane Hydroisomerization. *ACS catalysis* **2020**, *10* (23), 14245-14257.
- (19) Marinkovic, N. S.; Sasaki, K.; Adzic, R. R. Determination of single-and multi-component nanoparticle sizes by x-ray absorption spectroscopy. *Journal of The Electrochemical Society* **2018**, *165* (15), J3222.
- (20) Yang, T.; Feng, Y.; Ma, R.; Li, Q.; Yan, H.; Liu, Y.; He, Y.; Miller, J. T.; Li, D. Improvement of selectivity in acetylene hydrogenation with comparable activity over ordered PdCu catalysts induced by post-treatment. ACS Applied Materials & Interfaces 2020, 13 (1), 706-716.
- (21) Hadjiivanov, K.; Venkov, T.; Knözinger, H. FTIR Spectroscopic Study of CO Adsorption on Cu/SiO2: Formation of New Types of Copper Carbonyls. *Catalysis letters* **2001**, *75*, 55-59.
- (22) Ricciardulli, T.; Gorthy, S.; Adams, J. S.; Thompson, C.; Karim, A. M.; Neurock, M.; Flaherty, D. W. Effect of Pd Coordination and Isolation on the Catalytic Reduction of O_2 to H_2O_2 Over PdAu Bimetallic Nanoparticles. *Journal of the American Chemical Society* **2021**, *143* (14), 5445-5464.
- (23) Balkenende, A.; Van der Grift, C.; Meulenkamp, E.; Geus, J. Characterization of the surface of a Cu/SiO2 catalyst exposed to NO and CO using IR spectroscopy. *Applied surface science* **1993**, *68* (2), 161-171.
- (24) UV-Vis-NIR, D. Cu/SiO2 and Cu/SiO2-TiO2 Catalysts. *Journal of Catalysis* **1999**, *184*, 316-326.
- (25) Ouyang, M.; Papanikolaou, K. G.; Boubnov, A.; Hoffman, A. S.; Giannakakis, G.; Bare, S. R.; Stamatakis, M.; Flytzani-Stephanopoulos, M.; Sykes, E. C. H. Directing Reaction Pathways via In Situ Control of Active Site Geometries in PdAu Single-Atom Alloy Catalysts. *Nature Communications* **2021**. *12* (1), 1549.
- (26) Darby, M. T.; Sykes, E. C. H.; Michaelides, A.; Stamatakis, M. Carbon monoxide poisoning resistance and structural stability of single atom alloys. *Topics in catalysis* **2018**, *61* (5), 428-438.
- (27) Giannakakis, G.; Trimpalis, A.; Shan, J.; Qi, Z.; Cao, S.; Liu, J.; Ye, J.; Biener, J.; Flytzani-Stephanopoulos, M. NiAu Single Atom Alloys for the Non-Oxidative Dehydrogenation of Ethanol to Acetaldehyde and Hydrogen. *Topics in Catalysis* **2018**, *61*, 475-486.
- (28) Shan, J.; Liu, J.; Li, M.; Lustig, S.; Lee, S.; Flytzani-Stephanopoulos, M. NiCu Single Atom Alloys Catalyze the CH Bond Activation in the Selective Non-Oxidative Ethanol Dehydrogenation Reaction. *Applied Catalysis B: Environmental* **2018**, *226*, 534-543.
- (29) Shan, J.; Janvelyan, N.; Li, H.; Liu, J.; Egle, T. M.; Ye, J.; Biener, M. M.; Biener, J.; Friend, C. M.; Flytzani-Stephanopoulos, M. Selective Non-Oxidative Dehydrogenation of Ethanol to Acetaldehyde and Hydrogen on Highly Dilute NiCu Alloys. *Applied Catalysis B: Environmental* **2017**, *205*, 541-550.
- (30) Li, H.; Chai, W.; Henkelman, G. Selectivity for ethanol partial oxidation: the unique chemistry of single-atom alloy catalysts on Au, Ag, and Cu (111). *Journal of materials chemistry A* **2019**, *7* (41), 23868-23877.

- (31) Patel, D. A.; Giannakakis, G.; Yan, G.; Ngan, H. T.; Yu, P.; Hannagan, R. T.; Kress, P. L.; Shan, J.; Deshlahra, P.; Sautet, P. Mechanistic insights into nonoxidative ethanol dehydrogenation on NiCu single-atom alloys. *ACS Catalysis* **2023**, *13* (7), 4290-4303.
- (32) Davidson, J. M.; McGregor; Doraiswamy, L. The Mechanism of Palladium-Catalyzed Decomposition of Ethanol A Comparison of Chemical Kinetic and Surface Science Studies. *Industrial & engineering chemistry research* **2001**, *40* (1), 108-113.
- (33) Mavrikakis, M.; Barteau, M. A. Oxygenate Reaction Pathways on Transition Metal Surfaces. *Journal of Molecular Catalysis A: Chemical* **1998**, *131* (1-3), 135-147.
- (34) Stacchiola, D.; Calaza, F.; Burkholder, L.; Tysoe, W. T. Vinyl Acetate Formation by the Reaction of Ethylene With Acetate Species on Oxygen-Covered Pd (111). *Journal of the American Chemical Society* **2004**, *126* (47), 15384-15385.
- (35) Crathorne, E.; MacGowan, D.; Morris, S.; Rawlinson, A. Application of isotopic transient kinetics to vinyl acetate catalysis. *Journal of Catalysis* **1994**, *149* (2), 254-267.
- (36) Simson, S.; Jentys, A.; Lercher, J. A. Dynamic Self-Organization of Supported Pd/Au Catalysts during Vinyl Acetate Synthesis. *The Journal of Physical Chemistry C* **2013**, *117* (16), 8161-8169.
- (37) Trimble, R.; Brown, G. Copper (II) acetate monohydrate-An erroneous melting point. *Journal of Chemical Education* **1976**, *53* (6), 397.
- (38) Grennberg, H.; Foot, J. S.; Banwell, M. G.; Roman, D. S. Palladium(II) Acetate. In *Encyclopedia of Reagents for Organic Synthesis*, pp 1-35.
- (39) Zha, Z.; Deshlahra, P. Mechanistic Framework and Effects of High Coverage in Vinyl Acetate Synthesis. *ACS Catalysis* **2021**, *11* (3), 1841-1857. (40) Boerner, T. J.; Deems, S.; Furlani, T. R.; Knuth, S. L.; Towns, J. Access: Advancing innovation: Nsf's advanced cyberinfrastructure coordination ecosystem: Services & support. In *Practice and Experience in Advanced Research Computing*, 2023; pp 173-176.

TOC Graphic





VA synthesis reaction forms SAAs with high dispersion, reactivity and selectivity